ISSN 0036-0295, Russian Metallurgy (Metally), Vol. 2020, No. 11, pp. 1267–1275. © Pleiades Publishing, Ltd., 2020.
Russian Text © The Author(s), 2020, published in Metally, 2020, No. 6, pp. 31–40.

Powder Titanium Nickelide: Technology and Properties

A. V. Kasimtsev[a, *], G. V. Markova[b], S. S. Volodko[a, b, **], S. N. Yudin[a], B. V. Karpov[c], and I. A. Alimov[a, b]

[a] *OOO Metsintez, Tula, Russia*
[b] *Tula State University, Tula, Russia*
[c] *National University of Science and Technology MISiS, Moscow, Russia*
**e-mail: metsintez@yandex.ru*
***e-mail: volodko.sv@yandex.ru*

Received March 31, 2020; revised July 21, 2020; accepted July 27, 2020

Abstract—The influence of various schemes of thermomechanical treatment (TMT) on the structure and properties of two sintered nickel-rich binary TiNi powder alloys is shown. TMT is found to decrease the average grain size and to increase the strength characteristics, the alloy density, and the plasticity relative to the initial sintered state. The influence of TMT on the phase composition of the alloy is detected by X-ray diffraction. TMT is shown to promote the formation of the triclinic R-martensite or strain aging with the precipitation of the Ti_2Ni_3 phase.

Keywords: powder TiNi, structure, mechanical properties, deformation, thermomechanical treatment, density
DOI: 10.1134/S0036029520110087

INTRODUCTION

The alloys based on the TiNi intermetallic compound (titanium nickelide) demonstrate excellent functional properties (superelasticity, shape memory effect, damping ability) in combination with a good structural strength and corrosion resistance [1, 2]. Therefore, TiNi-based alloys are used in medicine and engineering for the manufacture of control or load-bearing elements of structures [3–9]. The functional properties of TiNi alloys are based on a reversible martensitic transformation (MT), the temperatures of which are extremely sensitive to changes in the chemical composition of the B2-phase and an alloy as a whole.

The main methods for producing titanium intermetallics and titanium nickelide are foundry methods, namely, vacuum-arc and vacuum-induction melting [10]. The properties of ingots, especially ingots of different heats, can differ significantly in composition and, hence, the critical MT temperatures. Therefore, it is necessary to study each piece of an ingot, which is practically impossible in mass production [11].

An analysis of the structure of as-cast ingots showed that, in addition to the main phase (high-temperature B2-phase or B2-phase + martensite), the ingots always contain foreign parasitic phases (Ti_2Ni, $TiNi_3$, Ti_4Ni_2O, etc.), the total content of which is variable, as a rule 5–20 wt % [11–13]. The formation of these phases is associated with segregation during ingot solidification and the interaction of a melt with oxygen in casting, which cannot be suppressed in large ingots.

A negative influence of the foreign phases, especially Ti_2Ni and Ti_4Ni_2O, on the plasticity and functional properties of TiNi-based alloys was detected [13, 14]. Therefore, the problem of developing new technologies to produce TiNi alloys of given chemical and phase compositions is challenging. The absence of foreign phases in a TiNi alloy is thought to eliminate the scatter of functional properties over the billet volume and to increase the mechanical characteristics.

This problem can be solved using powder metallurgy methods. As compared with the processes of traditional casting metallurgy (melting, solidification), powder metallurgy (synthesis of alloy powder + solid-phase sintering) has a number of advantages. The properties of cast metals and alloys are substantially determined by the peculiarities of their solidification, during which defects such as segregation (chemical) heterogeneity of the ingot composition, coarse grains with different sizes, contrast phase composition, and diffused interdendritic microporosity can form. A cast structure does not provide the expected functional and mechanical properties of the TiNi intermetallic compound. The correction of the structure requires long and multistage treatment of an as-cast material (homogenizing annealing, deformation, thermomechanical treatment (TMT)).

In turn, the compacted materials produced by powder metallurgy methods from fine powders are

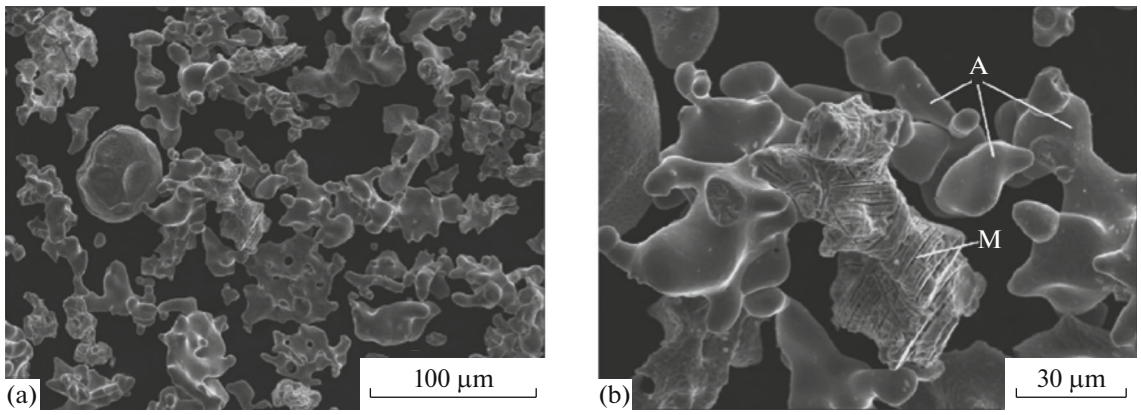

Fig. 1. SEM images of the TiNi intermetallic powder: (a) general view, (b) martensite relief on the powder surface (A, B2-phase; M, martensite) [20].

always subjected to consolidation, which is usually performed in a solid phase, i.e., at the temperatures not exceeding (0.9–0.95) T_m. In the powder metallurgy technology, it is possible to avoid all negative phenomena associated with ingot solidification. The advantages of powder metallurgy also include the possibility of forming workpieces with the shapes and sizes as close as possible to the requirements of the final product. There are other works devoted to the fabrication of titanium nickelide by powder metallurgy methods, such as SHS synthesis and reaction sintering (see, e.g., [15, 16]). However, in practice, these methods cannot always produce TiNi with homogeneous phase and chemical compositions.

In this work, we summarize the results of our works performed in recent years to fabricate high-quality semifinished products of powder titanium nickelide. The experimental powder technology developed for producing TiNi alloys [17, 18] includes the following main stages: calcium hydride synthesis of a powder TiNi alloy → powder consolidation by pressing and sintering → hot deformation for producing compact workpieces of specified sizes and shape.

CALCIUM HYDRIDE SYNTHESIS

The fabrication of metal and alloy powders by the joint reduction of oxide–metal mixtures by calcium hydride refers to metallothermic methods, in which calcium hydride is used as a reducing agent [19]. Schematically, the calcium hydride reaction of TiNi alloy powder synthesis can be represented as follows:

$$TiO_2 + Ni + 2CaH_2 \rightarrow TiNi + 2CaO + 2H_2\uparrow. \quad (1)$$

As a result of reaction (1), a sinter, namely, the reaction products in the form of intermetallic TiNi and CaO particles, forms. Evolved gaseous hydrogen burns during isothermal holding. Calcium oxide is removed by standard hydrometallurgical treatment operations (quenching, leaching).

TiNi powders were fabricated under experimental–industrial conditions [20]. Figure 1 shows the typical morphology of the calcium hydride TiNi powders. The chemical compositions of the powders of the two experimental batches are given in Table 1. Their phase compositions are as follows: batch 1, 100 vol % B2-phase; batch 2, 80% B2-phase + 10% R-martensite + 10% B19'-martensite. X-ray diffraction (XRD) analysis did not detect other (foreign) phases.

Table 1. Chemical composition of the intermetallic TiNi calcium hydride powders

Powder	Element content, wt %									
	main		impurity							
	Ni	Ti	C	Fe	Si	Co	N	O	H	Σ others
TN1 alloy (TU 1-809-394–84)	53.5–56.5	Base	<0.1	<0.3	<0.15	<0.2	<0.05	<0.2	<0.013	<0.3
TiNi: batch 1	55.5	″	0.067	0.1	0.02	–	0.015	0.1	0.30	Ca 0.13
batch 2	55.4	″	0.061	0.075	0.02	–	0.025	0.074	0.25	Ca 0.11

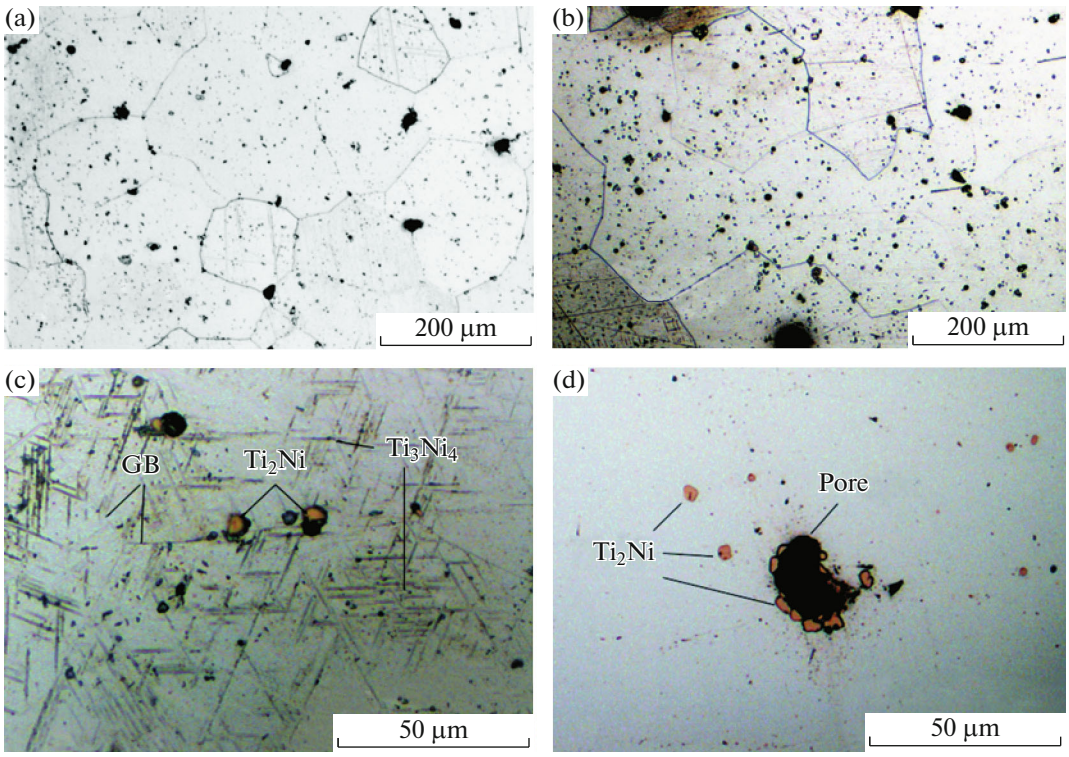

Fig. 2. Optical images of the structures of the bars fabricated by sintering of the powders of batch (a) 1 and (b–d) 2.

The content of the main elements (Ti, Ni) in the calcium hydride powders fully meet the requirements of TU 1-809-394–84 for the chemical composition of the TN1 cast alloy. Note that the powders of both batches were fabricated under the same technological conditions; in general, the hydride calcium technology makes it possible to produce similar TiNi intermetallic powder compositions.

The impurity composition is also important, since the mechanical, physical, and functional properties of the TiNi intermetallic compound depend substantially on impurity elements such as oxygen, carbon, nitrogen, and hydrogen, the content of which, with the exception of hydrogen, in TiNi powder alloys does not exceed the limits established by TU 1-809-394–84 on a cast TN1 alloy. The hydrogen content is adjusted to the required values at the subsequent stages of powder alloy consolidation. In addition, the powder production process can be improved to decrease the impurity content.

POWDER CONSOLIDATION

The authors of [20, 21] showed that hydrostatic forming (cold isostatic pressing) of a powder followed by vacuum sintering (vacuum of 0.013 Pa (10^{-4} mm Hg)) is the most preferred consolidation scheme, which is mainly due to the fact that gaseous impurities are partly removed from the material during vacuum sintering. The carbon and nitrogen content decreases by 15–30% in comparison with their content in the initial powder, the hydrogen content decreases by two orders of magnitude and does not exceed 0.003–0.004 wt % in the compacted sintered workpiece, and the decrease in the oxygen content is insignificant.

The photographs of the structures of the specimens after vacuum sintering were taken using a standard metallographic technique and an optical microscope (Fig. 2). This structure is represented by equiaxed straightened grains of the high-temperature B2-phase. There is a large number of junctions with a misorientation angle of 120°, which indicates recrystallization of the sintered material (Figs. 2a, 2b). However, a more detailed study of the structure showed that, in addition to B2-phase grains, a small number of secondary-phase needle inclusions (Fig. 2c) and standard-morphology inclusions (Figs. 2c, 2d) are present. As follows from the results of electron-probe microanalysis, the needle inclusions consist of the Ti_3Ni_4 phase and are uniformly distributed in the grain volume. The standard-morphology inclusions are represented by the Ti_2Ni phase, the presence of which is undesirable. In general, the parasitic Ti_2Ni phase content is so low that its presence is not determined by XRD. According to the results of metallographic studies, the parasitic-phase standard-morphology content varies in the range 0.5–1 vol % depending on the field of view. In Fig. 2c, the Ti_2Ni phase is located near a

grain boundary (GB). However, it should be noted that ~50% of the total Ti_2Ni phase content forms on the surface of isolated pores (see Fig. 2d). The formation of Ti_2Ni in the contact zone of the matrix material with pore boundaries is likely to be related to the formation of the η phase (Ti_4Ni_2O), which is the solid solution of oxygen in the Ti_2Ni lattice. The η phase in powdered titanium nickelide is thought to form in sintering due to the interaction of the matrix material with air in the pore volume. Oxygen was shown to stabilize the Ti_2Ni phase and its formation is possible in nickel-rich TiNi alloys [22].

EFFECT OF TMT ON THE STRUCTURE, DENSITY, AND MECHANICAL PROPERTIES OF TITANIUM NICKELIDE

Thermomechanical processing of the sintered TiNi powder alloy billets was carried out by rotary forging (RF), radial-shear rolling (RSR), and extrusion (Ex). For RF, the sintered workpieces had the following dimensions: the diameter was 15 mm, the length was 200–220 mm, and the density was 95–98% of the theoretical density ($\rho_t = 6.443$ g/cm^3). The RF temperatures were different (600, 900, 1000°C) and the true strain was $e = 0.628$ (bar diameter after deformation was 8 mm). We used an upgraded double-die rotary forging RKM2 B2129.02 machine.

For RSR, the dimensions of the sintered workpieces were as follows: the diameter was 33 mm and the length was 200 mm. RSR is a special case of screw rolling specially developed for the deformation of solid billets [23]. Due to high feed angles (18°–21°) and a specific roll pass design, this method can effectively deform solid billets with intensive grain refinement and compaction of the structure of various metals and alloys [24, 25]. For rolling bars of medium and small sections (10–50 mm), special minimills were designed and fabricated in MISiS [23]. In this work, rolling was carried out on two such three-high minimills (20–40 and 10–30) in two stages.

At the first stage, four passes were performed on mill 20–40 with a true strain $e = 0.095$, 0.318, 0.606, and 0.788 (bar diameters were 30, 24, 18, and 15 mm, respectively) per pass. The bar heating temperature for deformation was 1000°C. At the second stage, five passes with a true strain $e = 0.931$, 1.011, 1.098, 1.193, and 1.417 on a 10–30 mill were used to reach rod diameters of 13, 12, 11, 10, and 8 mm, respectively. The bar heating temperature for deformation was 900°C.

Extrusion was carried out on a P8041 horizontal hydraulic press with a maximum force of 12.5 MN (1250 tf). A container 80 mm in diameter and a die with a conical entry funnel (cone angle of 120°) and a hole diameter of 35 mm were used. The sintered billet sizes were as follows: the diameter was 78 mm and the length was 174 mm. Extrusion from an initial diameter of 80 mm into a rod 35 mm in diameter was carried out in one pass with a true strain $e = 0.801$ (reduction of 5.2). The heating temperature for deformation was 900°C and rods were cooled in air after all types of deformation. True strain e in all cases was estimated as the natural logarithm of the ratio of the initial bar diameter to the final diameter.

Depending on the type of TMT, we use the following abbreviations to describe the properties of specimens. For example, specimens RF900, RSR900, Ex900 are subjected to RF, RSR, and extrusion, respectively, at a temperature of 900°C.

The microstructures of the TiNi alloy subjected to TMT under various conditions were revealed by chemical etching of polished microsections with a reagent 1 part HF + 2 parts HNO_3 + 17 parts H_2O (see Fig. 3). An optical microscope with a built-in digital camera was used to take photographs. The structure of the RSR900 specimen could not be revealed by standard metallographic techniques; therefore, Electron Backscatter Diffraction technique (EBSD analysis) was used. Figure 3e shows the map of the crystallographic orientation distribution in the lattice.

The results of our study of the change in the structure and properties of powder TiNi during RF were published earlier [26]. The structure of the RF1000 and RF900 specimens is represented by polyhedral B2-phase grains with a large number of triple junctions with a misorientation angle of about 120° (Figs. 3a, 3b). A decrease in the RF temperature at the same strain ($e = 0.628$) promotes grain refinement (Table 2, $d_{av} = 92 \pm 7$ μm for the sintered specimen and 4 ± 1 μm for the RF600 specimen).

The formation of a fine-grained structure in the RF600 specimen (Fig. 3c) is likely to be related to the beginning of dynamic recrystallization [27, 28]. At deformation temperatures above 600°C, dynamic recrystallization proceeds actively and grain coarsening occurs more intensely. In the specimens after RF, a pronounced deformation structure with elongated grains is not observed.

The effect of RSR on the structure of powder TiNi was studied in detail in [29, 30]. Note that, in those works, we use the term helical rolling (HR); however, when screw rolling is used to form dense (pore-free) bars, it is correct to use the term RSR. When a significant strain ($e = 0.788$) is reached, the structure in the RSR1000 specimen is similar to that formed after RF at 900 and 1000°C (Fig. 3d). The grain boundaries are straightened, there are triple junctions with a misorientation angle of about 120°, and the grain shape is close to equilibrium. In comparison with the RSR1000 specimen, the RSR900 specimen ($e = 1.417$) has a small number of triple junctions (Fig. 3e), and the grains are slightly extended along the deformation direction. Moreover, the EBSD recrystallization maps showed that the total fraction of polygonized and

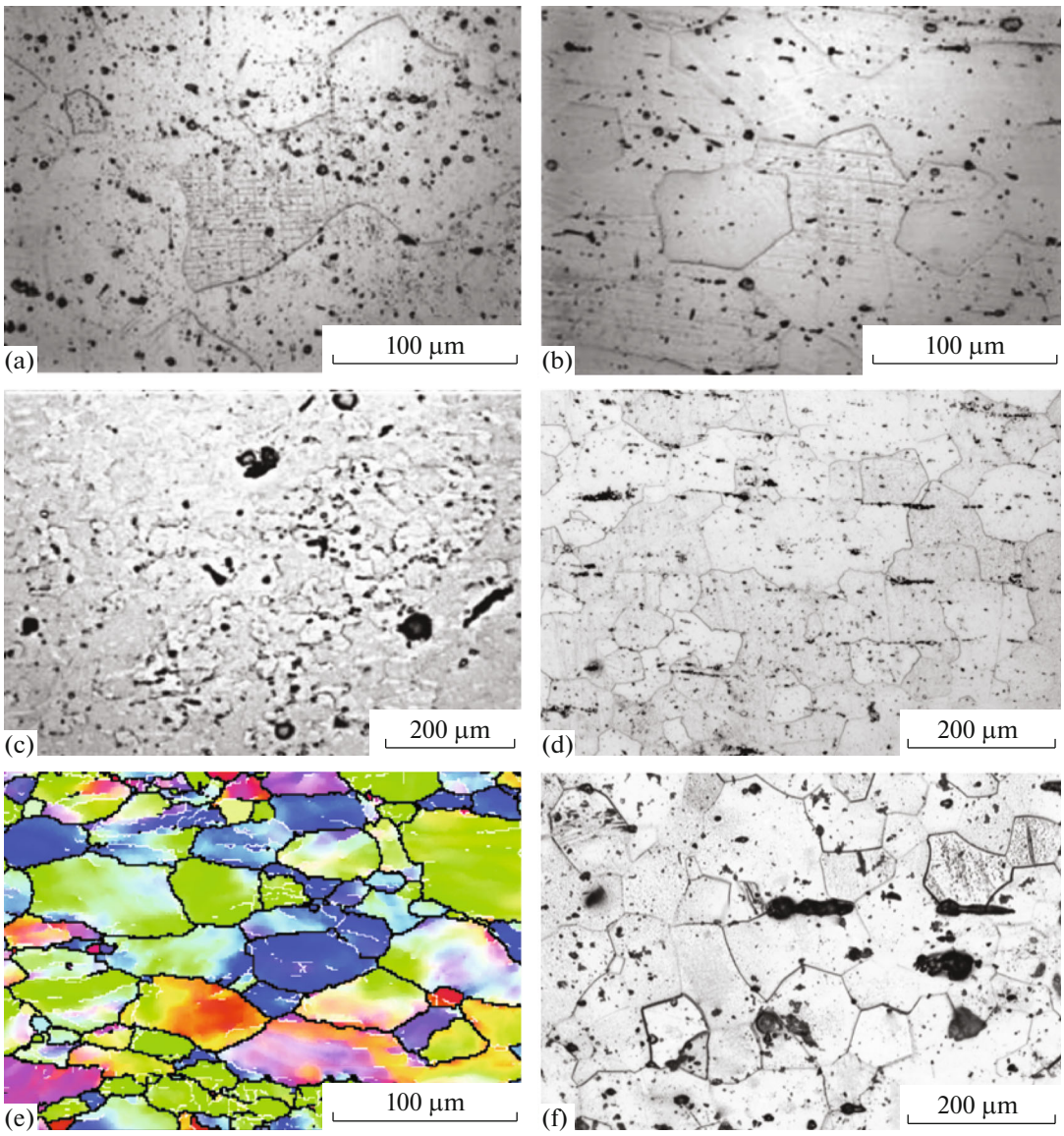

Fig. 3. Structure of the TiNi alloy after TMT along deformation: (a) RF1000, (b) RF900, (c) RF600, (d) RSR1000, (e) RSR900, and (f) Ex900.

recrystallized grains in the RSR900 specimen is only 7%, and the rest is the fraction of deformed grains.

RSR leads to grain refinement of the B2-phase. The average grain size begins to decrease only at $e = 0.606$ (see Table 2). The grain size in the RSR1000 specimen ($e = 0.788$) is $d_{av} = 64 \pm 2$ μm and that in the RSR900 specimen is 34 ± 2 μm. After RSR at 900°C ($e = 1.417$), the cross section of the deformed bar is characterized by different grain sizes, as is evidenced by a bimodal grain size distribution (Fig. 4). For the rest of the specimens, the type of grain size distribution corresponds to a lognormal distribution.

The fractions of polygonized (P), recrystallized (R), and deformed (D) grains at the periphery and the center of the bar are also different. We have P + R = 6% at the periphery and P + R ≈ 1% at the center. Therefore, the surface and central layers of the bar during RSR are deformed at different intensities. Hence, dynamic recrystallization develops nonuniformly over the cross section of the bar (more at the surface, less in the center), which leads to different fractions of recrystallized and polygonized grains and, hence, to a different grain sizes.

The extrusion of powder TiNi was studied in [31]. The structure formed in the Ex900 specimen after TMT during dynamic recrystallization consists of polyhedral B2-phase grains. The average grain size after extrusion (32 ± 2 μm) is almost 5 times smaller than in the initial sintered bar (150 ± 5 μm). In con-

Table 2. Mechanical properties and the grain sizes in the as-cast and powder TiNi alloys after sintering and TMT

TiNi alloy	t, °C	e	σ_u	$\sigma_{0.2}$	δ, %	E, GPa	HV	d_{av}, μm
			MPa					
As-cast deformed TU 1-809-253–80	–	–	539	294	>10	–	>140	–
Powder sintered:								
batch 1 (RF and RSR)	–	–	980	480	3.6	45	420 ± 15	92 ± 7
batch 2 (Ex)	–	–	1078	422	4.1	57	399 ± 4	150 ± 5
Powder, RF	1000	0.628	1120	890	5.4	62	391 ± 5	71 ± 7
	900	0.628	1390	600	14.5	53	398 ± 5	38 ± 4
	600	0.628	820	480	17.8	69	295 ± 4	4 ± 1
Powder, RSR	1000	0.095	–	–	–	–	365 ± 6	92 ± 3
	1000	0.318	–	–	–	–	386 ± 10	98 ± 3
	1000	0.606	–	–	–	–	400 ± 8	72 ± 4
	1000	0.788	1140	820	5.1	77	384 ± 8	64 ± 2
	900	1.417	1160	808	11.3	89	419 ± 7	34 ± 2
Powder, Ex	900	0.801	1250	780	13.1	68	419 ± 10	32 ± 2

t is the deformation temperature; HV, the microhardness; and d_{av}, the average grain size.

trast to RSR, extrusion and RF do not lead to different grain sizes over the cross section of the deformed bar.

As was found in [20, 21], sintered TiNi powder bars have residual porosity. Porosity is known to exert a significant effect on the inelastic behavior of titanium nickelide and, as a rule, to degrade the shape memory effect and superelasticity (SME, SE) [32]. Therefore, the maximum level of functional properties can be achieved in a nonporous material. The maximum SME and SE parameters can be used to apply titanium nickelide as a structural material with functional properties (actuators, dampers, etc.).

In this paper, TMT operations are considered to improve the functional and mechanical properties of powder TiNi by both refining the grain structure and reducing the residual porosity. The density after various TMT schemes was estimated by hydrostatic weighing according to GOST 18898–89 [33], and the results are presented in Fig. 5.

All TMT conditions used in this work were experimental and, in general, led to an increase in the density of the sintered powder bars. An exception is the RSR schedule during which tensile stresses were created in the central part of the bar at certain strains due to nonoptimal tool and deformation conditions for powder titanium nickelide; these stresses led to loosening of the metal in the core of the bar [29, 30].

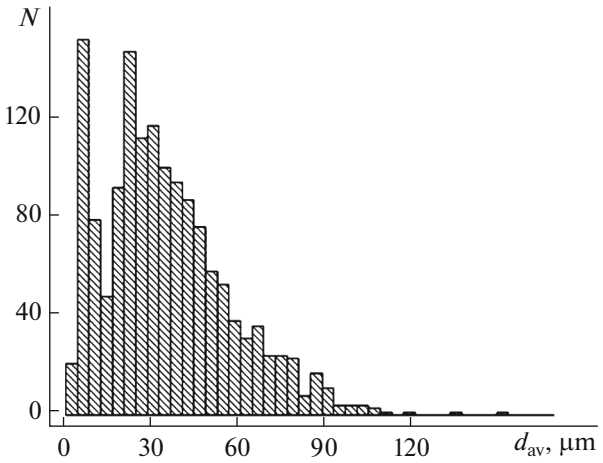

Fig. 4. Frequency diagram of the grain size distribution in the PVP900 specimen (N is the frequency).

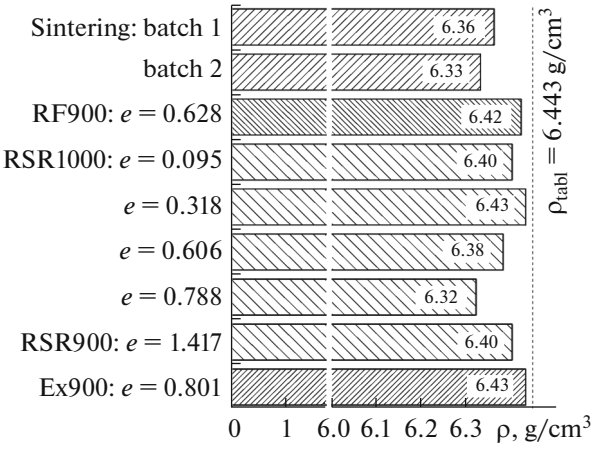

Fig. 5. Influence of TMT on the TiNi powder bar density ρ.

Table 3. Phase composition of the TiNi alloy fabricated by powder metallurgy

TiNi alloy, state		Fraction of phase, vol %			
		B2	R	B19	Ti_2Ni_3
Sintered state:	Batch 1 (RF and RSR)	100	–	–	–
	Batch 2 (Ex)	80	20	–	–
	RSR1000, $e = 0.095–0.788$	100	–	–	–
	RSR1000, $e = 0.788$	90	10	–	–
	RSR900, $e = 1.417$	95	5	–	–
	RF1000, $e = 0.628$	100	–	–	–
	RF900, $e = 0.628$	80	–	20	–
	RF600, $e = 0.628$	85	–	–	15
	Ex900, $e = 0.801$	100	–	–	–

An increase in the strain during RSR to $e = 1.417$ and a decrease in the rolling temperature to 900°C in the last stage led to an increase in the alloy density to 6.40 g/cm^3.

The mechanical properties were tested on an Instron 5581 tensile testing machine. Standard specimens were subjected to tensile tests in accordance with GOST 1497–84 at room temperature [34]. The sintered state of the alloy does not provide the required level of its plastic properties, which is required by TU 1-809-253–80 for hot-rolled bars of the TN1 cast alloy (see Table 2) because of the formation of a coarse-grained structure and porosity.

All types of TMT promote an increase in the strength and plasticity characteristics of powder TiNi not only to the required level, but also significantly higher. The maximum strength is provided by RF and Ex at 900°C, and the maximum plasticity is provided by RF at 600 and 900°C. The best complex of strength and ductility is reached after RF at 900°C ($e = 0.628$).

INFLUENCE OF TMT ON THE PHASE COMPOSITION OF THE TiNi ALLOY FORMED BY POWDER METALLURGY

The phase compositions of the alloy specimens were determined on a DRON-3 automated diffractometer using monochromatic Cu$K\alpha$ and Co$K\alpha$ radiation. X-ray diffraction patterns were recorded in the step scanning mode in the angle range $2\theta = 10°–110°$ for Cu$K\alpha$ radiation and 10°–145° for Co$K\alpha$ radiation at a step of 0.1° and a counting time of 4 s.

The results of quantitative phase analysis are given in Table 3. According to these data, the structure of the bar formed by sintering the powder of batch 1 is single-phase and consists of the high-temperature B2-phase. Insignificant disturbances are recorded at the angles of reflection corresponding to the R-phase; however, the amount of martensite cannot be reliably determined.

After RF at 1000°C, the structure is characterized by the presence of only the B2-phase. A decrease in the RF temperature to 900°C leads to the appearance of the trigonal martensitic R-phase (R-martensite). The appearance of this phase at room temperature is a consequence of an increase in the temperature of the reverse MT R $\rightarrow$ B2 above room temperature. After forging at 600°C, the Ti_2Ni_3 phase is found in the alloy structure, and its appearance can be due to aging caused by plastic deformation, as was noted in the case of cast titanium nickelide [27].

The results of XRD analysis showed that the alloy after RSR mainly has the structure of the B2-phase. After the first three passes, only traces of the trigonal (R) and orthorhombic (close to B19) martensite phases are found, and their amount, however, does not exceed the sensitivity of the method. After the fourth pass, the martensitic R-phase is reliably identified, the amount of which is not more than 10%. After the fifth pass to $e = 1.417$ at 900°C, the phase state B2 + R is retained in the structure.

The sintered bar made from the batch of powder 2 containing a lower amount of nickel was subjected to extrusion. In accordance with the concentration dependence of the MT points [35], a decrease in the nickel content causes an increase in the MT temperatures; as a result, the R-phase is detected in the initial powder in the sintered state. After extrusion, no reflections of the R and B19 martensite are observed, which can indirectly indicate a decrease in the MT temperatures.

Thus, TMT of sintered powder titanium nickelide leads to a certain change in the phase composition of the alloy due to a change in the ratio of the high-temperature (B2) to the martensitic (R) phases or in the chemical composition (change in the nickel content in

the two alloys under study) or due to a decrease in the TMT temperature.

CONCLUSIONS

(1) The laws of formation of the structure and properties of titanium nickelide fabricated by sintering of calcium hydride powders or by hot plastic deformation of various types, namely, RF, RSR, and extrusion, were studied by optical spectroscopy, XRD, and mechanical tests.

(2) All types of TMT were shown to change the structure of the alloy. During hot deformation, dynamic recrystallization and, hence, grain refining take place. Rotary forging at 900°C ($e = 0.628$), RSR with a final strain $e = 1.417$, or extrusion ($e = 0.801$) led to the formation of a structure with almost the same grain size ($d_{av} = 32–38$ μm). Forging at 600°C causes the formation of a fine-grained structure with a grain size $d_{av} = 4 \pm 1$ μm, and a structure with a grain size $d_{av} = 71 \pm 7$ μm forms at 1000°C.

(3) After TMT, the phase composition of the alloy weakly changed relative to the initial powder and the sintered state and consisted of either the B2-phase of the same chemical composition or the B2-phase and martensite. However, after rotary forging at 600°C, the Ti_2Ni_3 phase was found in the alloy structure, the appearance of which is due to aging caused by plastic deformation.

(4) As a result of TMT, the density of the powder sintered workpieces increases to an almost nonporous state. The maximum increase in the density relative to the sintered state is provided by extrusion. During RSR at $e > 0.318$, the axial zone of the rods undergoes loosening because of nonoptimal deformation conditions. An increase in the strain to $e = 1.417$ and a decrease in the RSR temperature of the TiNi powder alloy to 900°C in the last stage made it possible to reduce the porosity to 0.7% as compared to the initial porosity (~2%).

(5) All TMT technologies increase the relative elongation and the strength of the initial sintered bars. An exception is rotary forging at 600°C, which significantly increases the plasticity but lowers the ultimate strength relative to the sintered state. In the case of TMT at 900°C or below, the relative elongation of the TiNi powder specimens is ≥10%. The set of mechanical properties of the powder TiNi alloy in this case exceeds the level of requirements of TU 1-809-253–80 for hot-deformed cast alloy TN1 rods. The best set of the mechanical properties of the powder TiNi alloy was achieved after rotary forging at 900°C: $\sigma_u = 1390$ MPa, $\sigma_{0.2} = 600$ MPa, and $\delta = 14.5\%$.

REFERENCES

1. K. Otsuka and X. Ren, "Recent developments in the research of shape memory alloys," Intermetallics **273–275**, 134–148 (1999).
2. A. Misochenko et al., "Microstructure evolution and mechanical behavior in shape memory nanostructured TiNi alloy," Defect Diffus. Forum **385**, 169–174 (2018).
3. M. K. Ibrahim, E. Hamzah, S. N. Saud, and E. M. Nazim, "Powder metallurgy fabrication of porous 51 (at %) Ni–Ti shape memory alloys for biomedical applications," Shape Mem. Superelast. **4**, 327–336 (2018).
4. K. Kuribayashi, K. Tsuchiya, Z. You, et al., "Self-deployable origami stent grafts as a biomedical application of Ni-rich TiNi shape memory alloy foil," Mater. Sci. Eng. A **419**, 131–137 (2006).
5. G. Song, N. Ma, and H.-N. Li, "Applications of shape memory alloys in civil structures," Eng. Struct. **28**, 1266–1274 (2006).
6. D. Hartl, D. Lagoudas, J. Mabe, and F. Calkins, "Use of a Ni60Ti shape memory alloy for active jet engine chevron application. Part I," Thermomech. Charact. Smart Mater. Struct. **19**, 15–20 (2009).
7. E. Makino, T. Mitsuya, and T. Shibata, "Fabrication of TiNi shape memory micropump," Sensors and Actuators A: Phys. **88**, 256– 262 (2001).
8. J. Abadie, N. Chaillet, and C. Lexcellent, "Modeling of a new SMA micro-actuator for active endoscopy applications," Mechatronics **19**, 437–442 (2009).
9. S. V. Shishkin and N. A. Makhutov, *Calculation and Designing of Power Structures Based on Shape Memory Alloys* (Izhevsk, 2007).
10. Yu. K. Okunev, V. V. Rybin, and V. N. Slepnev, "Prospects for the development of production of cast billets from titanium alloys and its intermetallic compounds," Vopr. Materialoved., No. 4, 22–36 (2005).
11. M. Yu. Kollerov, A. V. Aleksandrov, D. E. Gusev, and A. A. Sharonov, "Influence of a charge material and a melting method on the structure and the shape memory effect of nickelide-based titanium alloy ingots," Tekhnol. Legkikh Splavov, No. 2, 87–93 (2012).
12. M. Yu. Kollerov, A. A. Il'in, I. S. Pol'kin, A. S. Fainbron, D. E. Gusev, and S. V. Khachin, "Structural aspects of the manufacture of semiproducts made from titanium nickelide–based alloys," Russ. Metall. (Metally), No. 5, 417–425 (2007).
13. N. N. Popov, T. I. Sysoeva, S. D. Prokoshkin, V. F. Larkin, and I. I. Vedernikov, "Mechanical properties and reactive stresses of Ti–Ni–Nb shape memory alloys," Russ. Metall. (Metally), No. 4, 317–325 (2007).
14. *Shape Memory Materials*, Ed. by K. Otsuka and C. M. Wayman (Cambridge University Press, Cambridge, 1998).
15. Yu. F. Yasenchuk and V. E. Gunter, "Influence of the initial combustion temperature on the micro- and macrostructure of titanium nickelide formed by SHS," Fundam. Problemy Sovr. Materialoved., No. 1, 24–28 (2005).
16. Yu. F. Yasenchuk, N. V. Artyukhova, and V. E. Gunter, "Reaction sintering of porous titanium nickelide and its

structure," Fundam. Problemy Sovr. Materialoved., No. 3, 11–16 (2010).

17. A. V. Kasimtsev, A. V. Shuitsev, and S. N. Yudin, "Method of fabricating TiNi-based alloy bars," RF Patent 2630740, 2017.
18. A. V. Kasimtsev, A. V. Shuitsev, G. V. Markova, and S. N. Yudin, "Method for fabricating a powder TiNi alloy with a high level of mechanical properties," RF Patent 2632047, 2017.
19. A. V. Kasimtsev and Yu. V. Levinskii, *Hydride–Calcium Powders of Metals, Intermetallics, Refractory Compounds, and Composite Materials* (Izd. MITKhT, Moscow, 2012).
20. A. V. Kasimtsev, G. V. Markova, A. V. Shuitsev, Yu. V. Levinskii, T. A. Sviridova, and A. V. Alpatov, "Powder hydride-calcium intermetallic TiNi," Izv. Vyssh. Uchebn. Zaved., Poroshk. Metallurg. Funkts. Pokryt., No. 3, 31–37 (2014).
21. A. V. Kasimtsev, G. V. Markova, A. V. Shuitsev, Yu. V. Levinskii, T. A. Sviridova, and A. V. Alpatov, "Changing a structure during the consolidation of calcium hydride powders of the TiNi intermetallic compound," Metallurg, No. 11, 108–114 (2014).
22. V. G. Chuprina and I. M. Shalya, "Reaction of TiNi with oxygen," Powder Met. Metal Ceram. **41**, 85–89 (2002).
23. S. P. Galkin, B. A. Romantsev, and E. A. Kharitono, "Putting into practice innovative potential in the universal radial-shear rolling process," CIS Iron Steel Rev. Jan. **2014** (9), 35–39 (2014).
24. B. V. Karpov, P. V. Patrin, S. P. Galkin, E. A. Kharitonov, and I. B. Karpov, "Radial-shear rolling of titanium alloy VT-8 bars with controlled structure for small diameter ingots (≤200 mm)," Metallurgist **61** (9–10), 884–890 (2018).
25. S. Dobatkin, S. Galkin, Y. Estrin, V. Serebryany, M. Diez, N. Martynenko, E. Lukyanova, and V. Perezhogin, "Grain refinement, texture, and mechanical properties of a magnesium alloy after radial-shear rolling," J. Alloys Compd. **774**, 969–979 (2019).
26. A. V. Kasimtsev, G. V. Markova, A. V. Shuytsev, T. A. Sviridova, and S. S. Volod'ko, "Changes in the structure and properties of powdered calcium hydride titanium nickelide during rotary forging," Tekhnol. Legkikh Splavov, No. 3, 44–52 (2016).
27. M. Yu. Kollerov, D. E. Gusev, A. V. Sharova, and A. V. Aleksandrov, "Structure formation in a TN1 alloy during deformation and heat treatment," Titan, No. 3, 4–10 (2010).
28. S. D. Prokoshkin, L. M. Kaputkina, S. A. Bondareva, O. Yu. Tikhomirova, L. P. Fatkullina, and S. V. Oleinikova, "Structure of hot-deformed austenite and properties of a Ti–Ni–Fe alloy after HTMT," Fiz. Met. Metalloved. **71** (3), 144–149 (1991).
29. G. V. Markova, A. V. Kasimtsev, S. S. Volod'ko, and B. B. Bubnenkov, "Influence of helical rolling on the structure and properties of powder TiNi. Part 1," Tsvetn. Met., No. 11, 75–82 (2018).
30. G. V. Markova, A. V. Kasimtsev, S. S. Volod'ko, and I. A. Alimov, "Influence of helical rolling on the structure and properties of powder TiNi. Part 2," Tsvetn. Met., No. 12, 75–81 (2018).
31. G. V. Markova, A. V. Kasimtsev, S. S. Volod'ko, S. N. Yudin, I. A. Alimov, S. S. Goncharov, and T. A. Sviridova, "Influence of extrusion of powder TiNi alloy on its structure and properties," Tekhnol. Legkikh Splavov, No. 3, 34–42 (2019).
32. B. Yuan, M. Zhu, and C. Y. Chung, "Biomedical porous shape memory alloys for hard-tissue replacement materials," Materials **11**, 1716 (2018).
33. *GOST 18898–89 (ISO 2738–87). Powder Products. Methods for Determining Density, Oil Content, and Porosity* (Izd. Standartov, Moscow, 1990).
34. *GOST 1497–84 (ISO 6892–84). Metals. Tensile Test Methods* (Standartinform, Moscow, 2008).
35. I. I. Kornilov, O. K. Belousov, and E. V. Kachur, *Titanium Nickelide and Shape Memory Alloys* (Nauka, Moscow, 1997).

Translated by K. Shakhlevich